




Maximal coin-walker entanglement in a ballistic quantum walkRong Zhang,^{1,2,*} Ran Yang ^{1,*} Jian Guo,¹ Chang-Wei Sun,¹ Jia-Chen Duan,¹ Heng Zhou,³ Zhenda Xie,^{1,†} Ping Xu,^{4,1,‡}
Yan-Xiao Gong ^{1,§} and Shi-Ning Zhu ¹¹*National Laboratory of Solid State Microstructure, School of Physics, School of Electronic Science and Engineering, and Collaborative Innovation Center of Advanced Microstructures, Nanjing University, Nanjing 210093, China*²*College of Electronic and Optical Engineering, Nanjing University of Posts and Telecommunication, Nanjing 210023, China*³*School of Information and Communication Engineering, University of Electronic Science and Technology of China, Chengdu 611731, China*⁴*Institute for Quantum Information and State Key Laboratory of High Performance Computing, College of Computing, National University of Defense Technology, Changsha 410073, China*

(Received 12 May 2020; revised 4 April 2022; accepted 7 April 2022; published 26 April 2022)

We report that the position-inhomogeneous quantum walk (IQW) can be utilized to produce the maximal high-dimensional entanglement while maintaining the quadratic speedup spread of the wave function. Our calculations show that the maximal coin-walker entanglement can be generated in any odd steps or asymptotically in even steps, and the nearly maximal entanglement can be obtained in even steps after 2. We implement the IQW by a stable resource-saving time-bin optical network, in which a polarization Sagnac loop is employed to realize the precisely tunable phase shift. Our approach opens up an efficient way for high-dimensional entanglement engineering as well as promotes investigations on the role of coin-walker interactions in QW-based applications.

DOI: [10.1103/PhysRevA.105.042216](https://doi.org/10.1103/PhysRevA.105.042216)**I. INTRODUCTION**

Quantum walk (QW) is the quantum version of classical random walk (CRW) [1], which is considered as a universal computational primitive [2–4]. The quantum walker can be in a coherent superposition of many possible position states, resulting in the ballistic transport, which is a quadratic speedup compared with the diffusive spread of CRW [5]. In particular, by adding control to QW dynamics, the inhomogeneous QW (IQW) can behave as a variety of transport features, including the ballistic behavior, super diffusion, and localization [6–9]. The IQW is also a powerful tool for investigating the interactions and dynamics of quantum particles [10,11], simulating of complex phenomena [12–16], and engineering of quantum states [17–28].

The evolution of a QW is a dynamical interaction process, resulting in the coin-walker entanglement, or called the coin-position entanglement, which was studied in a variety of QWs [18–27]. As spanned in a large number of position states, the entanglement is in a high-dimensional Hilbert space, and can be used to enhance the test of quantum fundamentals [29,30] and the performance in quantum communication [31,32] and computation [33–35]. In a particular case that the coin is another degree of freedom of the walker, it is called the hybrid entanglement, which is also a valuable resource in quantum information processing and has broad applications [36–42]. In addition, the ballistic spread and quantum entanglement

can be employed to improve the efficiency and performance of the quantum algorithms [5,35]. All these applications usually require an efficient way for maximal entanglement generation. The Hadamard QW though exhibits the ballistic transport, namely, the quadratic speedup, cannot reach the maximal coin-walker entanglement [19,20]. In contrast, whereas the maximal entanglement can be created asymptotically by introducing dynamical disorder [23,25], or after 10-step evolution via an optimal set of coin operations [26,27], these QWs can only behave subballistic transports with the decreased spread velocity. Up to now, the simultaneous realization of maximal entanglement and quadratic speedup in the QW has remained a challenge.

In this work, we utilize the position-inhomogeneous quantum walk (IQW) to produce the maximal entanglement after any odd steps or large even steps asymptotically, and the nearly maximal one can be obtained after 2-step evolution. Meanwhile, the constructive interference is preserved leading to the ballistic spread of the wave function in the high-dimensional Hilbert space. Thereby the coin can be correlated to the walker carrying more positions after the same steps evolution, in contrast to the previous schemes with subballistic spread. Further, we demonstrate our scheme by implementing the IQW with a high-stable time-bin-encoded optical network, in which a stable polarization Sagnac interferometer is developed to perform the precisely controlled position-dependent dynamics evolution. Based on the well-established equivalence of the evolution of coherent light in a linear optical network and that of a single photon (see p. 106 in [43]), here the dimmed pulse laser is employed to simulate the dynamic evolution of single photons [44–46] and this works because only the superposition principle is needed. We simultaneously observe the quadratic speedup transport and maximal entanglement entropy through the time-multiplexing

*These authors contributed equally to this work.

†xiezhen@nju.edu.cn

‡pingxu520@nju.edu.cn

§gongyanxiao@nju.edu.cn

measurement and the coin-state tomography. Our approach opens up an efficient way to engineer the maximal high-dimensional entanglement, which is applicable in a variety of different physical systems such as atoms [47], trapped ions [48,49], and photons [50,51].

II. MAXIMAL ENTANGLEMENT WITH CONSTRUCTIVE INTERFERENCE

A quantum walk is defined on a bipartite system composed of a quantum coin and a walker. The quantum coin is a two-level system with $|0\rangle$ ($|1\rangle$) dictating the left (right) moving direction of the walker for the next step. The position state of the walker at node x is expressed as $|x\rangle$ ($x \in \mathbb{Z}$). The evolution operator of the IQW is defined as

$$\hat{U} = \sum_x \hat{S}_x [\hat{C}(x) \otimes \hat{I}], \quad (1)$$

where \hat{I} is the identity operator on the walker and $\hat{C}(x)$ denotes the position-dependent coin operation. Here the coin operation performed at the position $x = 0$ is the product of the Hadamard operation and a phase shift

$$\hat{C}(0) = \frac{1}{\sqrt{2}} \begin{pmatrix} 1 & 1 \\ 1 & -1 \end{pmatrix} \begin{pmatrix} e^{i\phi} & 0 \\ 0 & e^{i\phi} \end{pmatrix}, \quad (2)$$

with $\phi \in [0, 2\pi)$. While at the other positions $x \neq 0$, $\hat{C}(x)$ is the Hadamard operation. Thus, this IQW becomes the Hadamard QW (HQW) when $\phi = 0$ is chosen. The state-dependent shift operation \hat{S}_x makes the walker move to the neighboring left (right) node determined by the coin state $|0\rangle$ ($|1\rangle$), which is expressed as

$$\hat{S}_x = |0\rangle\langle 0| \otimes |x-1\rangle\langle x| + |1\rangle\langle 1| \otimes |x+1\rangle\langle x|. \quad (3)$$

The nonlocal operation \hat{S}_x leads to the coin-walker entanglement.

We consider the initial coin-walker state is a localized state at the original position $x = 0$, written as

$$|\Psi(0)\rangle = [a(0, 0)|0\rangle + b(0, 0)|1\rangle]|0\rangle, \quad (4)$$

with the complex coefficients satisfying $|a(0, 0)|^2 + |b(0, 0)|^2 = 1$. After the t -step evolution described by $|\Psi(t)\rangle = \hat{U}^t |\Psi(0)\rangle$, the final state can be expressed as

$$|\Psi(t)\rangle = \sum_x [a(x, t)|0\rangle + b(x, t)|1\rangle]|x\rangle, \quad (5)$$

with $x = -t, -t+2, \dots, t-2, t$. The amplitudes $a(-1, t)$ and $b(1, t)$ can be calculated by

$$a(-1, t) = \frac{1}{\sqrt{2}} e^{i\phi} [a(0, t-1) + b(0, t-1)], \quad (6)$$

$$b(1, t) = \frac{1}{\sqrt{2}} e^{i\phi} [a(0, t-1) - b(0, t-1)], \quad (7)$$

and the other amplitudes derived from $x \neq 0$ are

$$a(x-1, t) = \frac{1}{\sqrt{2}} [a(x, t-1) + b(x, t-1)], \quad (8)$$

$$b(x+1, t) = \frac{1}{\sqrt{2}} [a(x, t-1) - b(x, t-1)]. \quad (9)$$

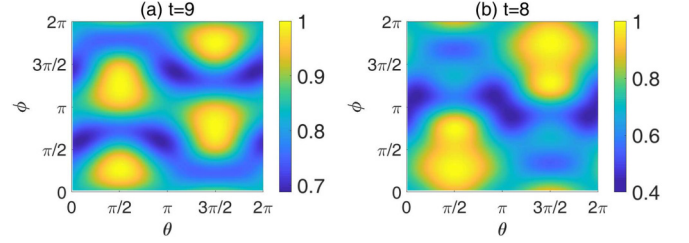


FIG. 1. The von Neumann entropy of the coin-walker entanglement E as a function of the initial state parameter θ and the coin operation parameter ϕ of the inhomogeneous quantum walk for the steps of (a) $t = 9$ and (b) $t = 8$.

It is clear that we have $\sum_x |a(x, t)|^2 + |b(x, t)|^2 = 1$ due to the normalized condition.

The evolved coin-walker state remains pure as a result of the unitary evolution together with the pure initial state, so the entanglement of $|\Psi(t)\rangle$ can be quantified through the von Neumann entropy. The von Neumann entropy is defined as $E(\rho_c) = -\text{Tr}(\rho_c \log_2 \rho_c)$ with 1 and 0 for the maximally entangled and separable states, respectively, where $\rho_c(t)$ is the reduced density matrix of coin state obtained by the partial trace over the walker state $\text{Tr}_P[|\Psi(t)\rangle\langle\Psi(t)|]$. According to the state given by Eq. (5), we obtain

$$\rho_c = \begin{pmatrix} A(t) & C(t) \\ C(t)^* & B(t) \end{pmatrix}, \quad (10)$$

with $A(t) = \sum_x |a(x, t)|^2$, $B(t) = \sum_x |b(x, t)|^2$, and $C(t) = \sum_x a(x, t)b(x, t)^*$. Then the von Neumann entropy is calculated by

$$E(\rho_c) = -\lambda_1 \log_2 \lambda_1 - \lambda_2 \log_2 \lambda_2, \quad (11)$$

where $\lambda_{1,2}$ are two eigenvalues of ρ_c expressed as

$$\lambda_{1,2} = \frac{1}{2} \{1 \pm \sqrt{1 + 4[|C(t)|^2 - A(t)B(t)]}\}. \quad (12)$$

A necessary condition of obtaining the maximal entanglement is that the two diagonal matrix elements of ρ_c equal $1/2$ [20], and hence here we choose a typical balanced state as the initial state which is given by

$$|\Psi(0)\rangle = \frac{1}{\sqrt{2}} (|0\rangle + e^{i\theta}|1\rangle)|0\rangle, \quad (13)$$

with $\theta \in [0, 2\pi)$. Therefore, we have $A(t) = B(t) = 1/2$ and $\lambda_{1,2} = 1/2 \pm |C(t)|$. So the entanglement entropy E depends on the initial state, coin operations, and evolution steps.

Then we investigate the von Neumann entropy as a function of θ and ϕ for any step with the amplitude recursion formulas given by Eqs. (6) to (9). Taking $t = 9$ and $t = 8$ for example, the calculation results are shown in Figs. 1(a) and 1(b), respectively. We can see that the maximal value of the von Neumann entropy can be obtained by choosing $\phi = \pi/4$, $\theta = \pi/2$, or $\phi = 7\pi/4$, $\theta = 3\pi/2$. Actually, the two conditions can maximize the von Neumann entropy for all the steps except step 2. Taking either condition, here choosing the first one, we plot the entanglement entropy for 60 steps in Fig. 2(a), and list the von Neumann entropy values for 11 steps in Table I (column $E_{\text{IQW}}^{\text{theo}}$). It is shown that for any odd steps, maximal entanglement $E = 1$ can be obtained, while for the

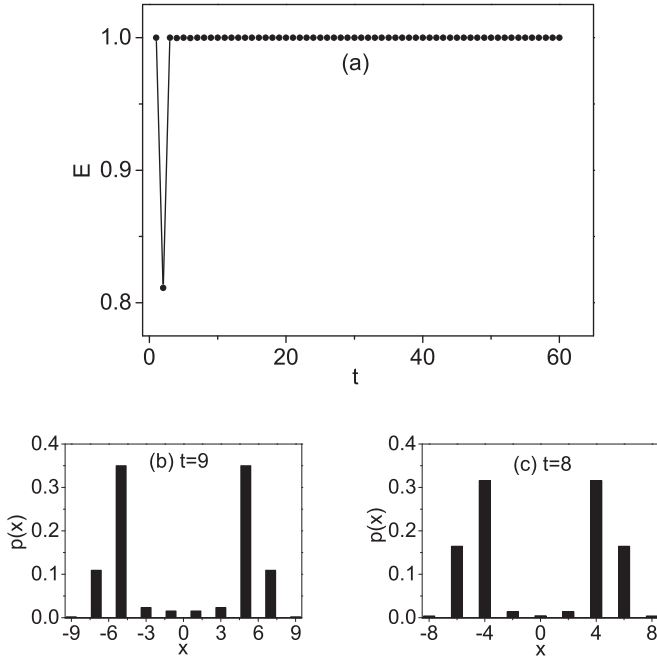


FIG. 2. In the IQW with $\theta = \pi/2$ and $\phi = \pi/4$, the von Neumann entropy E as a function of evolution step t and the actual dimension can be confirmed by the nonzero probabilities of $t + 1$ positions such as $t = 9$ and $t = 8$.

even steps, the maximal entanglement is achieved asymptotically and nearly maximal entanglement with $E > 0.99$ has been achieved since step 2. For comparison, we also list the von Neumann entropy values for the HQW in Table I (column $E_{\text{HQW}}^{\text{theo}}$), which are all around 0.87. The actual dimension of the maximal coin-walker entangled state in the IQW is $2 \times (t + 1)$ because the coin state is in a two-dimensional Hilbert space as shown in Eq. (10) and the walker is spanned in $t + 1$ -dimensional position space $\{|x\rangle\}$ with $x = -t, -t + 2, \dots, t$ after the evolution of t steps. The dimension of the walker can be confirmed by the nonzero probabilities of positions and the examples of $t = 9$ and $t = 8$ are shown in Figs. 2(b) and 2(c), respectively.

TABLE I. Experimental results and theoretical values of the von Neumann entropy of the inhomogeneous quantum walk (IQW) and the Hadamard quantum walk (HQW). Errors are estimated from the statistical errors.

Step	$E_{\text{IQW}}^{\text{theo}}$	$E_{\text{IQW}}^{\text{exp}}$	$E_{\text{HQW}}^{\text{theo}}$	$E_{\text{HQW}}^{\text{exp}}$
1	1	0.99 ± 0.01	1	0.99 ± 0.01
2	0.81128	0.86 ± 0.01	0.811	0.81 ± 0.01
3	1	0.99 ± 0.01	0.811	0.81 ± 0.01
4	0.99967	0.95 ± 0.02	0.896	0.88 ± 0.02
5	1	0.95 ± 0.02	0.896	0.88 ± 0.02
6	0.99967	0.99 ± 0.02	0.857	0.83 ± 0.02
7	1	0.99 ± 0.02	0.857	0.86 ± 0.02
8	0.99999	0.97 ± 0.03	0.882	0.90 ± 0.02
9	1	0.99 ± 0.04	0.882	0.89 ± 0.03
10	0.99999	0.99 ± 0.05	0.865	0.88 ± 0.04
11	1	0.99 ± 0.06	0.865	0.85 ± 0.05

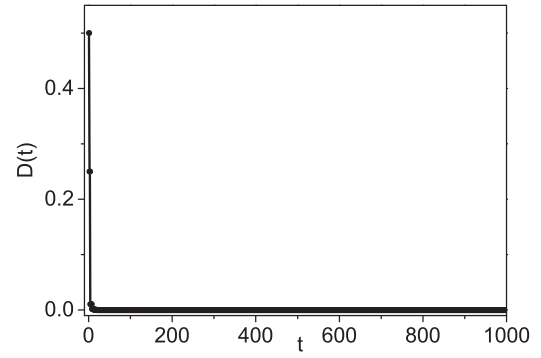


FIG. 3. Trace distance between two neighboring coin states as a function of evolution step t with $\theta = \pi/2$ and $\phi = \pi/4$.

To further investigate the asymptotic limit of entanglement in even steps, we calculate the trace distance between two coin states in adjacent steps by

$$D(t) = \frac{1}{2} \text{Tr}[|\rho_c(t) - \rho_c(t-1)|], \quad (14)$$

where $|M| = \sqrt{M^\dagger M}$ for a matrix M . For the qubit state $\rho_c(t)$, the trace distance $D(t)$ is equal to the Ky Fan 1-norm, i.e., the largest singular value of $\rho_c(t) - \rho_c(t-1)$ [52]. In Fig. 3, we plot the calculation results of $D(t)$ in up to 1000 steps and then get a nonlinear fitting function of $D(t) \sim t^{-1.90}$. Consequently, we have $\lim_{t \rightarrow \infty} [\rho_c(t+1) - \rho_c(t)] = 0$. Namely, $\rho_c(t+1) = \rho_c(t)$ works in the large step regime. As for any odd steps maximal entanglement is obtained, and hence maximal entanglement is achieved in the large even step regime as well.

The signature of quantum effects is also imaged in the walker's spread velocity quantified by the position variance $v(t) = \langle x^2 \rangle - \langle x \rangle^2$. We show the calculation results of the position variance for the above IQW up to 1000 steps in Fig. 4 (the black solid curve), and for comparison the position variance values of the HQW (the red dashed curve) and CRW (the blue dotted line) are given as well. One can see that the IQW and HQW can both exhibit the ballistic transport due to the maintained constructive interference, in contrast to the diffusive spread of CRW. Moreover, the IQW spreads even faster than the HQW.

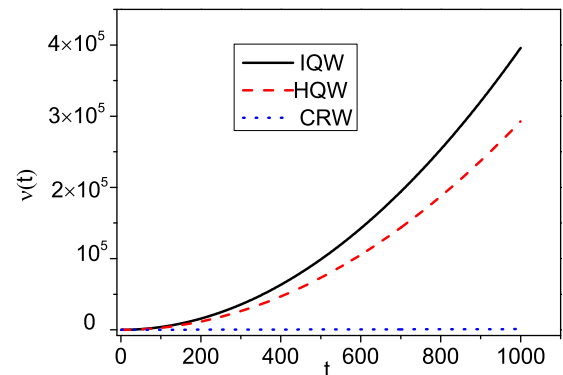


FIG. 4. Position variance as a function of evolution step t with $\theta = \pi/2$ and $\phi = \pi/4$.

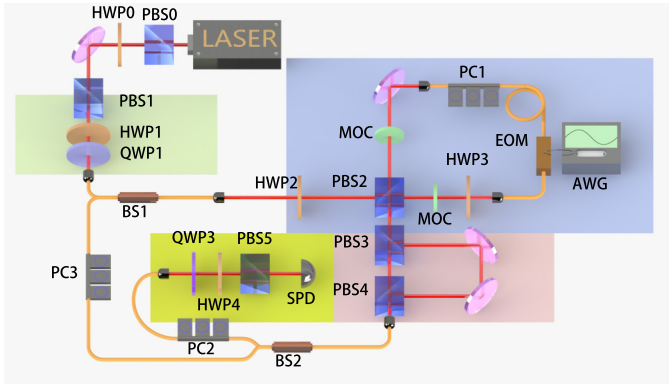


FIG. 5. Experimental setup of the ordered inhomogeneous quantum walk. PBS: polarization beam splitter; HWP: half-wave plate; QWP: quarter-wave plate; BS: single-mode fiber beam splitter; PC: polarization controller; MOC: magneto-optic crystal; EOM: electro-optic phase modulator; AWG: arbitrary wave generator; SPD: single-photon detector.

III. EXPERIMENTAL DEMONSTRATIONS

We realize the IQW defined in Eqs. (1) to (3) by the resource-saving time-bin encoded optical network as sketched in Fig. 5. Our setup consists of three parts, the initial state preparation (the green part), the evolution (the blue and pink parts), and the state measurement (the yellow part). The horizontal and vertical polarization states $|H\rangle$ and $|V\rangle$ represent the coin states $|0\rangle$ and $|1\rangle$, respectively. The position states are encoded in discrete time bins formed by distinct path lengths. We use an electromodulated picosecond diode laser (Hamamatsu Photonics, PLP-10), with a pulse width of 70 ps, a repetition rate of 1 MHz, and a central wavelength of 1550 nm. The laser output first passes through a polarization beam splitter (PBS0), a half-wave plate (HWP0), PBS1 and the light intensity can be controlled by tuning the optical axis angle of the HWP0. Then the light is coupled into the evolution of quantum walk via the $1/99$ port of a $1:99$ single-mode fiber beam splitter (BS1) after passing through HWP1 and the quarter-wave plate (QWP1), where the two wave-plates can prepare an arbitrarily initial polarization of the light output from BS1.

The evolution of a single-step IQW is realized by a round trip through the optical network including the variable coin operations (the blue part) and state-dependent shift operator (the pink part). The position-dependent coin operations given in Eq. (2) are realized through HWP2 followed by a polarization Sagnac loop. Explicitly, the optical axis of HWP2 is oriented at 22.5° to perform the Hadamard operation. Because the phase modulations generated directly by the electro-optic phase modulator (EOM) (Eospace) depend on H and V polarizations with the restriction $\phi_V/\phi_H = 3.5$, the Sagnac loop in the blue part of Fig. 5 is employed to perform two respective fast-tunable phase shifts ϕ_V , ϕ_H on the H and V polarization of the input light in a stable way. First, a beam of light is input from one port of PBS2, and the H and V polarization parts are separated into counterclockwise and clockwise paths, respectively. Second, the input port of clockwise light is fused with a single-mode fiber to introduce

a 39.1-ns delay of the arrival time at the EOM compared with the counterclockwise light, so that the phases on H and V polarization can be precisely controlled by the voltages on the EOM separately. Both ports of the EOM are connected by polarization-maintaining (PM) fibers in a slow aligned axis. A magneto-optic crystal (MOC) is placed in each path to make the polarization rotate 45° counterclockwise. The optical axis of HWP3 is tuned to make the diagonal polarization coupling with the slow axis of the PM fiber. Likewise, the polarization controller PC1 is adjusted to couple the antidiagonal polarization with the slow axis. Finally, the EOM was triggered by a programmable electric pulse output from the arbitrary wave generator (AWG) (Tektronix, AWG7012), and the light in each path returns its original polarization with an individual modulated phase at the output of the loop. Here the required phases on H and V polarization are the same $\phi_V = \phi_H = \pi/4$ as shown in Eq. (2).

The shift operation \hat{S}_x given in Eq. (3) is implemented by an unbalanced polarization Mach-Zehnder interferometer formed by PBS3 and PBS4, where the V polarization is delayed $\Delta t = 2.3$ ns compared with the H polarization. The temporal difference Δt corresponds to a step in two positions $x \pm 1$. Finally, about one percent of photons are coupled out of the network to the measurement setup and the majority go to the next round of the network via a $99:1$ beam splitter BS2, with a one-loop time of $T = 72.9$ ns. The one-loop loss is measured to be 3.6 dB. The measurement setup consists of a single-photon detector (SPD) (Quintique id201) and a combination of QWP3, HWP4, and PBS5, which can realize any state projection measurement [53,54]. The SPD and the laser are both triggered by the electrical pulses from the AWG. Therefore, the state evolution of each step can be accurately monitored in our setup. All experimental results are averaged over more than 10^4 detected events.

The initial coin-walker state at the original position is prepared as $|\Psi_1(0)\rangle = (|H\rangle + i|V\rangle)|0\rangle/\sqrt{2}$. As shown in Eqs. (1) to (3), we realize the HQW and IQW by choosing $\phi = 0$, and $\pi/4$, respectively. For the HQW, the EOM is powered off. To implement the required IQW, the phase shift $\phi_V = \phi_H = \pi/4$ on both H and V polarizations are performed at the position $x = 0$ of even steps $2m$ corresponding with the time bins of $t_0 = m(2T + \Delta t)$ ($m \in \mathbb{Z}$). So a programmable electrical pulses from the AWG with a pulse width of 1 ns and a pulse height of 1.8 V at both time bins t_0 and $t_0 + 39.1$ ns is applied on the EOM when the H polarization pulse and the V one of the position $x = 0$ arrive.

After t -step evolution, the initial light pulses with the time bin $t = 0$ are distributed in $t + 1$ time windows corresponding with the positions $x = -t, -t + 2, \dots, t$. We apply projecting measurement on the polarization bases $\{|H\rangle, |V\rangle, |H\rangle + |V\rangle, |H\rangle - i|V\rangle\}$ for each time bin. So we obtain the position distribution probabilities by adding up the counts of projection measurement on state $|H\rangle$ and $|V\rangle$ in each position, and then normalizing them with the sum of all the positions. The experimental results of IQW (red bars) and HQW (yellow bars) in step 11 are shown in Fig. 6, with the black and blue bars representing the corresponding theoretical probabilities, respectively. The position distributions for both HQW and IQW clearly show the non-Gaussian behaviors of the completely coherent quantum walks. To compare the experimental

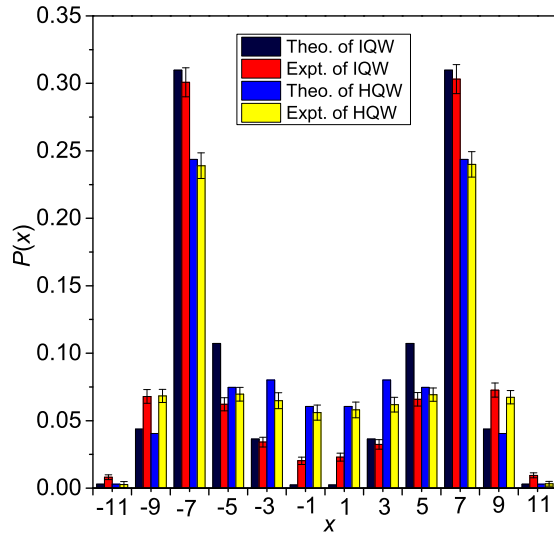


FIG. 6. Experimental and theoretical position distributions $P(x)$ of the inhomogeneous quantum walk (IQW) and the Hadamard quantum walk (HQW) in step 11. Error bars are simulated from the statistical errors.

(P_{exp}) and theoretical (P_{theo}) distributions, we employ the fidelity defined by $S = \sum_x \sqrt{P_{\text{exp}} P_{\text{theo}}}$, which ranges from 0 for the complete mismatch to 1 for the perfect concordance. The fidelities for HQW and IQW after the 11-step evolution are calculated as $S_H = 0.9805 \pm 0.0002$ and $S_I = 0.9673 \pm 0.0002$, respectively. Therefore, nearly perfect coherence in our setup is confirmed by the non-Gaussian distributions after the 11-step evolution. Particularly, the fidelities of the final position distributions of the maximal entanglement as a function of dimensions $t + 1$ are shown in Fig. 7.

Based on the experimental results of the position distributions of the two types of QWs, we calculated the position variance $v(t) = \sum_x P(x, t) |x - \mu(t)|^2$ with $\mu(t) = \sum_x P(x, t)x$ to quantify the spread of the wave function. The variance of the HQW (blue triangle) and IQW (red circle) in up to 11 steps is shown in Fig. 8, with the corresponding theoretical results plotted as the red solid curve and the blue dotted curve. For comparison, the variance of CRW is also

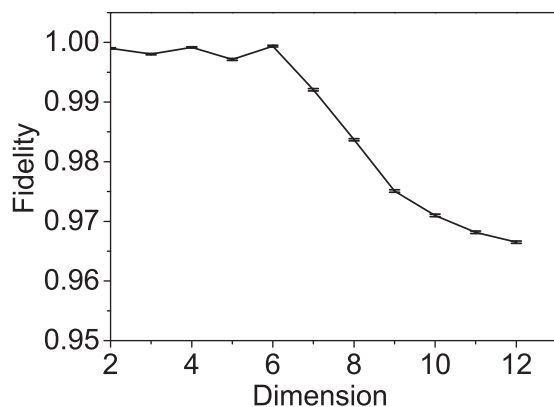


FIG. 7. The fidelities of IQW featured with the maximal entanglement as a function of dimensions. Error bars are simulated from the statistical errors.

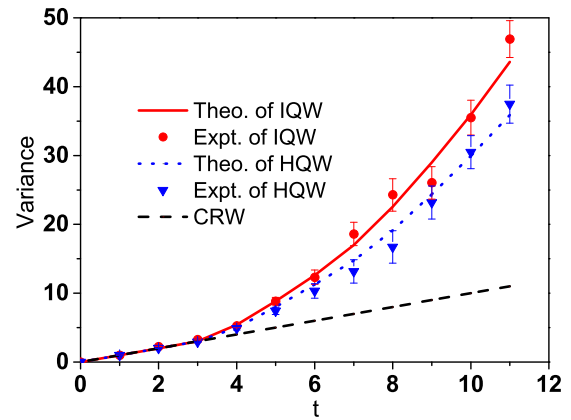


FIG. 8. Experimental position variance against the evolution step t for the inhomogeneous quantum walk (IQW), the Hadamard quantum walk (HQW) in up to 11 steps, with the corresponding theoretical solid curves. The black solid curve represents the theoretical position variance of the classical random walk (CRW). Error bars are simulated from the Poissonian statistics.

plotted with the black dashed curve. We can see that, in contrast to the diffusive spread in CRW, the IQW as well as the HQW can behave the quadratic speedup spread, and moreover, the IQW spreads even faster than the HQW. Taking step 11 as an example, the position variances of the IQW, HQW, and CRW are $v_I(11) = 46.91 \pm 2.99$, $v_H(11) = 37.46 \pm 2.76$, and $v_C(11) = 11$, respectively.

The above experimental results, including both the non-Gaussian distribution and quadratic speedup, demonstrated that the coherence are maintained perfectly and further confirm that the coin walker is in the coherent superposition state during the whole evolution [55]. We also employ the normalized linear entropy (NLE) [56,57] to estimate the purity of the coin-walker state directly. NLE is defined as $N(\rho) = \frac{d}{d-1} [1 - \text{Tr}(\rho^2)]$ with d is the dimension of system, and $N(\rho) = 0$ for pure states and 1 for completely mixed states. We first calculated the lowest bound of $\text{Tr}(\rho^2)$ with the coin-walker state ρ . Then the coin state at every position of two neighboring steps can be obtained by projecting corresponding light pulses on measurement basis $\{|H\rangle, |V\rangle, |H\rangle + |V\rangle|H\rangle - |iV\rangle\}$. We can obtain partial entries of the coin-walker density matrix by the experimental results. Then the disciplined convex programming toolbox of the MATLAB software [58] is employed to achieve the lowest value of $\text{Tr}(\rho^2) = 0.900 \pm 0.082$ based on the properties of density matrix including Hermitian, unity trace and nonnegative eigenvalues. So we obtain $N(\rho) \leq 0.105 \pm 0.071$, which experimentally certifies the coin-walker state is a nearly pure state.

So the von Neumann entropy can be used to quantify the coin-walker entanglement. The state tomography on the reduced coin density matrix can be obtained by adding up the counts of all $t + 1$ positions for each bases polarization state $\{|H\rangle, |V\rangle, |H\rangle + |V\rangle|H\rangle - |iV\rangle\}$. And we reconstruct all the coin density matrices from step 1 to 11 of the HQW and IQW, respectively. The fidelities, calculated by $F = (\text{Tr} \sqrt{\sqrt{\rho_c^{\text{exp}}} \rho_c^{\text{theo}} \sqrt{\rho_c^{\text{exp}}}})^2$, are all higher than $F_H = 0.967 \pm 0.008$ and $F_I = 0.952 \pm 0.009$ for HQW and IQW,

respectively. The calculated values of the von Neumann entropy from the experimental results are listed in Table I, which all agree well with the corresponding theoretical values. Therefore, it is experimentally shown that the maximal coin-walker entanglement can be produced in the ballistic quantum walk.

IV. CONCLUSION

We proposed and experimentally demonstrated that the position-inhomogeneous quantum walk (IQW) can generate maximal coin-walker entanglement as well as behave in the quadratic speedup by employing position-dependent coin operations. Our theoretical analysis showed that maximal coin-walker entanglement can be created in any odd steps or asymptotically in even steps, and approximately maximal entanglement can be generated in even steps after 2 as well. We implemented the IQW through a stable time-bin-walking optical network, with a fast-tunable polarization Sagnac loop

developed for implementing the coin operations. We observed high-fidelity evolutions in up to 11 steps and both the maximal entanglement and quadratic speedup in the IQW were confirmed experimentally. Our approach opens up a way for efficient creation of high-dimensional (hybrid) entanglement, which has applications in a variety of quantum technologies. Our investigations can be extended to high-dimensional QW with broader applications. Our work can also prompt the applications such as quantum computation based on the quantum walk with respect to the role of coin-walker interactions.

ACKNOWLEDGMENTS

This work was supported by the National Key R&D Program of China (Grants No. 2019YFA0705000 and No. 2019YFA0308700), the Key R&D Program of Guangdong Province (Grant No. 2018B030329001), and the National Natural Science Foundation of China (Grants No. 51890861, No. 11547031, No. 11705096, No. 11674169, No. 11627810, No. 61705033, No. 11690031, and No. 11974178).

-
- [1] Y. Aharonov, L. Davidovich, and N. Zagury, Quantum random walks, *Phys. Rev. A* **48**, 1687 (1993).
- [2] A. M. Childs, Universal Computation by Quantum Walk, *Phys. Rev. Lett.* **102**, 180501 (2009).
- [3] A. M. Childs, D. Gosset, and Z. Webb, Universal computation by multi-particle quantum walk, *Science* **339**, 791 (2013).
- [4] Y. Lahini, G. R. Steinbrecher, A. D. Bookatz, and D. Englund, Quantum logic using correlated one-dimensional quantum walks, *npj Quantum Inf.* **4**, 2 (2018).
- [5] J. Kempe, Quantum random walks: an introductory overview, *Contemp. Phys.* **44**, 307 (2003).
- [6] A. K. Schreiber, K. N. Cassemiro, V. Potoček, A. Gábris, I. Jex, and Ch. Silberhorn, Decoherence and Disorder in Quantum Walks: From Ballistic Spread to Localization, *Phys. Rev. Lett.* **106**, 180403 (2011).
- [7] A. Gerdardi, A. Laneve, L. D. Bonavena, L. Sansoni, J. Ferraz, A. Fratallocchi, F. Sciarrino, Á. Cuevas, and P. Mataloni, Experimental Investigation of Superdiffusion via Coherent Disordered Quantum Walks, *Phys. Rev. Lett.* **123**, 140501 (2019).
- [8] A. Wójcik, T. Łuczak, P. Kurzyński, A. Grudka, T. Gdala, and M. B. Bzdega, Trapping a particle of a quantum walk on the line, *Phys. Rev. A* **85**, 012329 (2012).
- [9] A. Schreiber, K. N. Cassemiro, V. Potoček, A. Gábris, P. J. Mosley, E. Andersson *et al.*, Photons Walking the Line: A Quantum Walk with Adjustable Coin Operations, *Phys. Rev. Lett.* **104**, 050502 (2010).
- [10] A. Schreiber, A. Gábris, P. P. Rohde, K. Laiho, M. Štefaňák, V. Potoček *et al.*, A 2D quantum walk simulation of two-particle dynamics, *Science* **336**, 55 (2012).
- [11] A. Crespi, R. Osellame, R. Ramponi, V. Giovannetti, R. Fazio, L. Sansoni *et al.*, Anderson localization of entangled photons in an integrated quantum walk, *Nat. Photonics* **7**, 322 (2013).
- [12] T. Kitagawa, M. A. Broome, A. Fedrizzi, M. S. Rudner, E. Berg, I. Kassal *et al.*, Observation of topologically protected bound states in photonic quantum walks, *Nat. Commun.* **3**, 882 (2012).
- [13] L. Xiao, X. Zhan, Z. H. Bian, K. K. Wang, X. Zhang, X. P. Wang *et al.*, Observation of topological edge states in parity-time-symmetric quantum walks, *Nat. Phys.* **13**, 1117 (2017).
- [14] S. Barkhofen, L. Lorz, T. Nitsche, Ch. Silberhorn, and H. Schomerus, Supersymmetric Polarization Anomaly in Photonic Discrete-Time Quantum Walks, *Phys. Rev. Lett.* **121**, 260501 (2018).
- [15] C. Chen, X. Ding, J. Qin, Y. He, Y. H. Luo, M. C. Chen, C. Liu, X. L. Wang, W. J. Zhang, H. Li *et al.*, Observation of Topologically Protected Edge States in a Photonic Two-Dimensional Quantum Walk, *Phys. Rev. Lett.* **121**, 100502 (2018).
- [16] X. Y. Xu, Q. Q. Wang, W. W. Pan, K. Sun, J. S. Xu, G. Chen *et al.*, Measuring the Winding Number in a Large-Scale Chiral Quantum Walk, *Phys. Rev. Lett.* **120**, 260501 (2018).
- [17] T. Giordani, E. Polino, S. Emiliani, A. Suprano, L. Innocenti, H. Majury *et al.*, Experimental Engineering of Arbitrary Qudit States with Discrete-Time Quantum Walks, *Phys. Rev. Lett.* **122**, 020503 (2019).
- [18] I. Carneiro, M. Loo, X. Xu, M. Girerd, V. Kendon, and P. L. Knight, Entanglement in coined quantum walks on regular graphs, *New J. Phys.* **7**, 156 (2005).
- [19] G. Abal, R. Siri, A. Romanelli, and R. Donangelo, Quantum walk on the line: Entanglement and nonlocal initial conditions, *Phys. Rev. A* **73**, 042302 (2006).
- [20] A. Romanelli, Distribution of chirality in the quantum walk: Markov process and entanglement, *Phys. Rev. A* **81**, 062349 (2010).
- [21] C. Di Franco, M. Gettrick, and Th. Busch, Mimicking the Probability Distribution of a Two-Dimensional Grover Walk with a Single-Qubit Coin, *Phys. Rev. Lett.* **106**, 080502 (2011).
- [22] S. Salimi and R. Yosefjani, Asymptotic entanglement in 1D quantum walks with a time-dependent coined, *Int. J. Mod. Phys. B* **26**, 1250112 (2012).
- [23] R. Vieira, E. P. M. Amorim, and G. Rigolin, Dynamically Disordered Quantum Walk as a Maximal Entanglement Generator, *Phys. Rev. Lett.* **111**, 180503 (2013).

- [24] R. Vieira, E. P. M. Amorim, and G. Rigolin, Entangling power of disordered quantum walks, *Phys. Rev. A* **89**, 042307 (2014).
- [25] Q. Q. Wang, X. Y. Xu, W. W. Pan, K. Sun, J. S. Xu, G. Chen *et al.*, Dynamic-disorder-induced enhancement of entanglement in photonic quantum walks, *Optica* **5**, 1136 (2018).
- [26] A. Gratsea, M. Lewenstein, and A. Dauphin, Generation of hybrid maximally entangled states in a one-dimensional quantum walk, *Quantum Sci. Technol.* **5**, 025002 (2020).
- [27] A. Gratsea, F. Metz, and T. Busch, Universal and optimal coin sequences for high entanglement generation in 1D discrete time quantum walks, *J. Phys. A: Math. Theor.* **53**, 445306 (2020).
- [28] Z. Yan, Y. Zhang, M. Gong, Y. Wu, Y. Zheng, S. Li *et al.*, Strongly correlated quantum walks in 12-qubit superconducting processor, *Science* **364**, 753 (2019).
- [29] T. Vértesi, S. Pironio, and N. Brunner, Closing the Detection Loophole in Bell Experiments Using Qudits, *Phys. Rev. Lett.* **104**, 060401 (2010).
- [30] N. Brunner, D. Cavalcanti, S. Pironio, Va. Scarani, and S. Wehner, Bell nonlocality, *Rev. Mod. Phys.* **86**, 419 (2014).
- [31] X. S. Liu, G. L. Long, D. M. Tong, and F. Li, General scheme for superdense coding between multiparties, *Phys. Rev. A* **65**, 022304 (2002).
- [32] A. Grudka and A. Wójcik, Symmetric scheme for superdense coding between multiparties, *Phys. Rev. A* **66**, 014301 (2002).
- [33] H. J. Briegel, D. E. Browne, W. Dür, R. Raussendorf, and M. Van den Nest, Measurement-based quantum computation, *Nat. Phys.* **5**, 19 (2009).
- [34] E. T. Campbell, Enhanced Fault-Tolerant Quantum Computing in d -Level Systems, *Phys. Rev. Lett.* **113**, 230501 (2014).
- [35] S. D. Berry and J. B. Wang, Two-particle quantum walks: entanglement and graph isomorphism testing, *Phys. Rev. A* **83**, 042317 (2011).
- [36] O. Morin, J. D. Bancal, M. Ho, P. Sekatski, and N. Sangouard, Witnessing Trustworthy Single-Photon Entanglement with Local Homodyne Measurements, *Phys. Rev. Lett.* **110**, 130401 (2013).
- [37] J. T. Barreiro, T. C. Wei, and P. G. Kwiat, Beating the channel capacity limit for linear photonic superdense coding, *Nat. Phys.* **4**, 282 (2008).
- [38] D. Llewellyn, Y. Ding, I. I. Faruque, S. Paesani, and M. G. Thompson, Chip-to-chip quantum teleportation and multiphoton entanglement in silicon, *Nat. Phys.* **16**, 148 (2020).
- [39] K. S. Choi, H. Deng, J. Laurat, and H. J. Kimble, Mapping photonic entanglement into and out of a quantum memory, *Nature (London)* **452**, 67 (2008).
- [40] S. P. Walborn, S. Pádua, and C. H. Monken, Hyperentanglement-assisted Bell-state analysis, *Phys. Rev. A* **68**, 042313 (2003).
- [41] C. Simon, M. Żukowski, H. Weinfurter, and A. Zeilinger, Feasible “Kochen-Specker” Experiment with Single Particles, *Phys. Rev. Lett.* **85**, 1783 (2000).
- [42] M. Michler, H. Weinfurter, and M. Żukowski, Experiments Towards Falsification of Noncontextual Hidden Variable Theories, *Phys. Rev. Lett.* **84**, 5457 (2000).
- [43] H. Paul, *Introduction to Quantum Optics: From Light Quanta to Quantum Teleportation* (Cambridge University Press, Cambridge, England, 2004).
- [44] B. Sephton, A. Dudley, G. Ruffato, F. Romanato, L. Marrucci, M. Padgett, S. Goyal, F. Roux, Th. Konrad, and A. Forbes, A versatile quantum walk resonator with bright classical light, *PLoS One* **14**, e0214891 (2019).
- [45] A. Regensburger, Ch. Bersch, B. Hinrichs, G. Onishchukov, A. Schreiber, Ch. Silberhorn, and U. Peschel, Photon Propagation in a Discrete Fiber Network: An Interplay of Coherence and Losses, *Phys. Rev. Lett.* **107**, 233902 (2011).
- [46] J. Boutari, A. Feizpour, S. Barz, C. Di. Franco, M. S. Kim, W. S. Kolthammer, and I. A. Walmsley, Large scale quantum walks by means of optical fiber cavities, *J. Opt.* **18**, 094007 (2016).
- [47] M. Karski, L. Forster, J. M. Choi, A. Steffen, W. Alt, D. Meschede *et al.*, Quantum walk in position space with single optically trapped atoms, *Science* **325**, 174 (2009).
- [48] S. H. Schmitz, R. Matjeschk, C. Schneider, J. Glueckert, M. Enderlein, T. Huber *et al.*, Quantum Walk of a Trapped Ion in Phase Space, *Phys. Rev. Lett.* **103**, 090504 (2009).
- [49] F. Zähringer, G. Kirchmair, R. Gerritsma, E. Solano, R. Blatt, and C. F. Roos, Realization of a Quantum Walk with One and Two Trapped Ions, *Phys. Rev. Lett.* **104**, 100503 (2010).
- [50] L. Sansoni, F. Sciarrino, G. Vallone, P. Mataloni, A. Crespi, R. Ramponi *et al.*, Two-Particle Bosonic-Fermionic Quantum Walk via Integrated Photonics, *Phys. Rev. Lett.* **108**, 010502 (2012).
- [51] H. Tang, X. F. Lin, Z. Feng, J. Y. Chen, J. Gao, K. Sun, *et al.*, Experimental two-dimensional quantum walk on a photonic chip, *Sci. Adv.* **4**, eaat3174 (2018).
- [52] M. A. Nielsen and I. L. Chuang, *Quantum Computation and Quantum Information* (Cambridge University Press, Cambridge, England, 2000).
- [53] D. F. V. James, P. G. Kwiat, W. J. Munro, and A. G. White, Measurement of qubits, *Phys. Rev. A* **64**, 052312 (2001).
- [54] F. Elster, S. Barkhofen, T. Nitsche, J. Novotný, A. Gábris, I. Jex *et al.*, Quantum walk coherences on a dynamical percolation graph, *Sci. Rep.* **5**, 13495 (2015).
- [55] T. A. Brun, H. A. Carteret, and A. Ambainis, Quantum to Classical Transition for Random Walks, *Phys. Rev. Lett.* **91**, 130602 (2003).
- [56] S. Bose and V. Vedral, Mixedness and teleportation, *Phys. Rev. A* **61**, 040101(R) (2000).
- [57] N. A. Peters, T. C. Wei, and P. G. Kwiat, Mixed-state sensitivity of several quantum-information benchmarks, *Phys. Rev. A* **70**, 052309 (2004).
- [58] CVX Research, Inc. M. C. Grant, and S. P. Boyd, CVX is a Matlab-based modeling system for convex optimization, <http://cvxr.com/cvx/>.